

DOI: 10.1002/cctc.201300072

Activity, Recyclability, and Stability of Lipases Immobilized on Oil-Filled Spherical Silica Nanoparticles with Different Silica Shell Structures

Yasutaka Kuwahara,^[a] Takato Yamanishi,^[a] Takashi Kamegawa,^[a] Kohsuke Mori,^[a, b] and Hiromi Yamashita^{*[a, b]}

Candida antarctica lipase A was immobilized on spherical silica nanoparticles with oil-filled core and oil-induced mesoporous silica shell with different silica shell structures. The immobilization of enzymes was achieved by directly adding enzymes to the oil-in-water emulsion system under ambient synthesis conditions, and the silica shell structure was controlled by the addition of the cosolvent ethanol to the initial synthesis medium. Detailed structural analysis revealed the formation of oil-filled spherical silica nanoparticles with 3.4–4.2 nm mesopores ran-

domly arranged in the silica shell; the thickness and pore characteristics of these pores markedly changed with the addition of ethanol. The retention of the enzyme activity during biocatalysis was significantly affected by the structural properties of the silica shells, and it was found that a thick and dense silica shell is essential to afford an active, recyclable, and stable biocatalyst. Furthermore, the oil encapsulated within the core cavity was found to play an important role in achieving a high catalytic efficiency.

Introduction

Since the initial discovery of synthetic routes to ordered mesostructured silicate materials, tremendous efforts have been directed toward the development of synthetic approaches for fabricating inorganic materials with controlled composition, hierarchical structure, and multifunctionalities.^[1–7] The use of mesostructured silicate materials produced by using the surfactant-induced self-assembly approach as hosts or carriers for biocatalysts has been of great interest in a wide range of applications in biochemistry, such as drug-delivery systems,^[8] biosensors,^[8,9] and enzymatic catalysis.^[10,11] A fundamental motivation for the use of mesostructured silicate materials is to stabilize biocatalysts by maintaining their fragile structural conformations and inherent enzymatic activities and improve their reusability, objectives to which they are ideally suited owing to their tunable structures (e.g., through morphology, porosity, and surface area) and high chemical stability.^[10–12]

To date, various synthetic strategies have emerged for hosting enzymes in cavities or onto silicate materials. The overwhelming majority for enzyme immobilization is chemical or physical fixation within the pore channels of functionalized mesoporous silica^[9–26] or onto the void cavities of silica-based macrocellular foam,^[27,28] the pore diameters of which are approximate to, or more than, the molecular diameter of enzymes because they offer rigid, uniform open pore structures and large pore volumes; however, the leaching of enzymes is suspicious, and the robust confinement of enzymes is not guaranteed in these open-ended silicate supports. Although the uptake of enzymes and their stabilities can be improved by enforcing the interactions between enzymes and the silicate surfaces by using the chemical modification techniques,^[12–20,27–30] the complicated synthetic methods, coupled with the high cost of these materials, limit their applicability on the industrial scale. The design of high-performance heterogeneous biocatalysts through a facile and scalable immobilization approach, by keeping the manufacturing cost low, still remains a challenge.

Of various silica-based host materials, silica hollow spheres have been envisaged as promising carriers for biomolecules owing to the presence of silica shell that functions as a physical barrier to protect them from the surrounding environment and a void volume to accommodate various guests.^[31–33] For example, Fujiwara et al. succeeded in directly encapsulating biomolecules (bovine serum albumin and duplex DNA) within the silica hollow spheres adopting an interfacial reaction by using a multiple (W₁/O/W₂) emulsion system.^[34] However, the integrity of biomolecule properties upon the encapsulation has been unclear. The direct addition of enzymes during the synthesis of silicate materials seems to be an inexpensive, operationally

[a] Dr. Y. Kuwahara,[†] T. Yamanishi, Dr. T. Kamegawa, Dr. K. Mori, Prof. Dr. H. Yamashita
Division of Materials and Manufacturing Science
Graduate School of Engineering
Osaka University
2-1, Yamada-oka, Suita, Osaka 565-0871 (Japan)
Fax: (+81) 6-6879-7457
E-mail: yamashita@mat.eng.osaka-u.ac.jp

[b] Dr. K. Mori, Prof. Dr. H. Yamashita
Unit of Elements Strategy Initiative for Catalysts & Batteries
Kyoto University
Katsura, Kyoto 615-8510 (Japan)

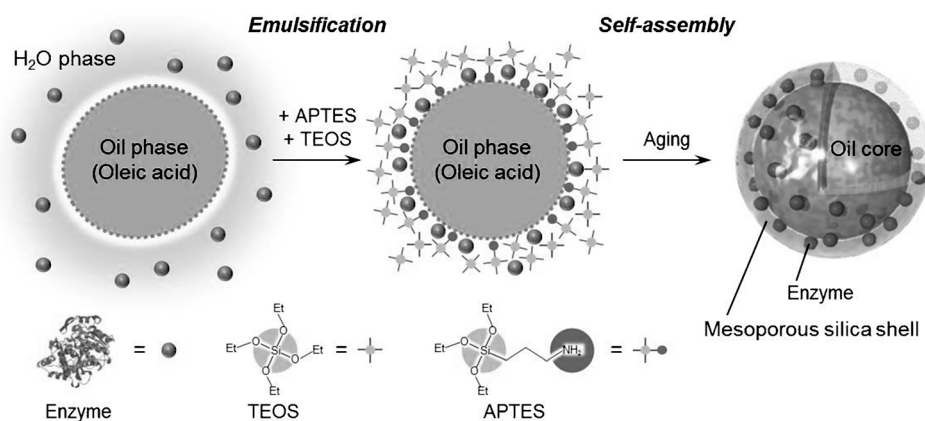
[†] Present address:
Research Institute for Innovation in Sustainable Chemistry
National Institute of Advanced Industrial Science and Technology (AIST)
16-1 Onogawa, Tsukuba, Ibaraki 305-8569 (Japan)

Supporting information for this article is available on the WWW under <http://dx.doi.org/10.1002/cctc.201300072>.

simple, and extremely versatile route for fabricating enzyme–silica composite biocatalysts; however, the synthetic methodology sometimes requires intricate multiple preparation steps and careful control of the synthetic conditions to circumvent the denaturation of enzymes.^[35,36]

The alternative strategy is their encapsulation inside sol-gel-derived silica matrices. These materials (designated as silica-coated enzymes) improve stabilities on enzymes because silica matrices function to efficiently protect the enzymes from the surrounding environment (e.g., pH and temperature) and against the denaturation/leaching of enzymes during catalytic operations owing to the robust confinement effect.^[37–42] However, most studies showed lower specific activity than that of the free enzymes owing to the problems associated with low diffusion rates and slow reaction kinetics derived from its nonporous structure. Thus, the silica coating of enzymes to improve their stabilities is not commensurate with good accessibility. The key to design high-performance enzyme–silica composite biocatalysts is likely an optimization of the accessibility between the reactive surface and the enzymes via a precise control over the location of enzymes.

We recently reported a novel synthetic protocol for immobilizing enzymes within spherical silica nanoparticles via an anionic surfactant-induced self-assembly approach and demonstrated that the resultant enzyme–silica composites act as efficient heterogeneous biocatalysts in both aqueous and organic solvents.^[43] In comparison with the prototypical composite biocatalysts without a hierarchical core–shell structure, such as enzymes impregnated on mesoporous silicas and silica-coated enzymes, the oil-filled silica nanoparticles (OSNs) with a unique core–shell structure that we have developed are promising supports for enzymes owing to the following fascinating features: 1) ambient synthetic conditions that preserve the inherent activity of enzymes, 2) a direct entrapment of enzymes via a facile preparation route, which largely simplifies the manufacturing process, 3) a stabilizing effect endowed by the silica shell, which enables increased stability and recyclability of enzymes, and 4) an optimized configuration of enzymes in the vicinity of the reactive silica shell surface, which facilitates the access of reactants.^[43] The overall synthesis process of enzyme-immobilized OSNs is illustrated in Scheme 1. In this synthetic approach, oleic acid (OA), an anionic surfactant with a carboxylic acid group, immersed in water is emulsified initially by an amino group of 3-aminopropyl triethoxysilane (APTES) with opposite charges, which self-assembles afterward to form mesoporous silica shell through a localized polymerization of silicon precursors (APTES and tetraethoxyorthosilicate [TEOS]) at the water–oil interface, and the enzymes are sequestered selectively within the silica matrix of the shell.^[44] Although the as-syn-



Scheme 1. A formation mechanism of enzyme-immobilized oil-filled silica nanoparticles.

thesized enzyme–silica composite was found to act as an efficient, recyclable, and stable biocatalyst, the optimization of its structure to maximize the catalytic activity of enzymes had not been conducted. Some key questions related to the structural optimization are as follows: 1) How is the silica shell structure most suitable for efficiently immobilizing enzymes? 2) Is the presence of oil in the core truly favorable for catalysis? 3) Is the immobilized enzyme active and stable toward an applied process? For example, the addition of specific amount of ethanol (EtOH) in the sol–gel process of mesoporous silica has a significant effect on the silicate structures (e.g., particle size and porosity) owing to the ability of EtOH to suppress the hydrolysis and condensation rate of TEOS^[45] and to reduce the surfactant packing parameter g .^[44] An extensive exploration of suitable structures of this composite biocatalyst may drastically change the activity, recyclability, and stability of enzymes and may provide constructive insights into the strategy for designing high-performance enzyme–silica composite biocatalysts.

We have examined activity, recyclability, and stability of the enzymes immobilized on OSN materials with different silica shell structures and investigated the relationships between the structures of the silicate support and the performances of the immobilized enzymes. Similar to our previous report,^[43] *Candida antarctica* lipase A (*Cal-A*) was used as a model enzyme throughout this work because it is one of the most recognized biocatalysts in a broad range of synthetic applications of industrial importance, such as kinetic resolutions, aminolysis, esterification, and transesterification reactions.^[28,46–48] The amount of EtOH added during the synthesis was varied to give the final products with different silica shell structures. The effect of EtOH on enzyme properties was investigated by monitoring change in pH during the syntheses and by comparing infrared spectra. The structures such as morphology, particle size, and porosity of the *Cal-A*-immobilized OSNs (*Cal-A@OSN*) were carefully investigated by using SEM, TEM, XRD, and nitrogen adsorption–desorption analysis. The residual enzyme activity, recyclability, and thermal/chemical stability of the composite biocatalysts were assessed by using the hydrolysis of *n*-butyl acetate in water as a test reaction. Furthermore, the effect of

the presence of oil (OA) on the enzyme activity was investigated.

Results and Discussion

Effect of EtOH on enzymes

As described in the Experimental Section, the immobilization of *Cal-A* was performed by directly adding enzymes to the initial emulsion system composed of OA, water, and EtOH. After the addition of silicon sources (TEOS and APTES), the resulting solution was aged for 24 h at 50 °C to yield silica networks. A higher hydrolysis and condensation rates of silicon sources can undoubtedly be obtained at a higher temperature; however, more moderate synthetic temperature, 50 °C, was adopted here to circumvent denaturation of the enzymes by heat.

Another important factor that potentially affects enzyme properties is change in pH during synthesis. The pH profiles obtained during the synthesis of *Cal-A*@OSN(0) and *Cal-A*@OSN(110) are shown in Figure 1. The solution containing

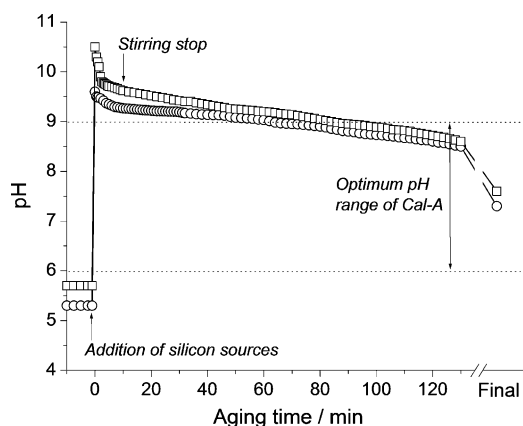


Figure 1. pH Profiles of the synthesis of *Cal-A*@OSN(0) (○) and *Cal-A*@OSN(110) (□).

Cal-A was initially at pH 5.3 for *Cal-A*@OSN(0), which increased instantaneously to pH 9.7 after the addition of silicon sources, followed by a gradual decrease along with aging. The lowest and highest pH values were slightly out of the permissible pH range of *Cal-A* (the optimum pH range for *Cal-A* is ≈ 6 –9 at room temperature)^[48]; however, it was found to decrease below pH 9 within 60 min and finally approached neutral, in which *Cal-A* can remain enzymatically active. Such ambient synthetic conditions would have little damage on the enzyme structures, which enables for an efficient entrapment of enzymes into their silica networks without affecting enzyme activities. On the other hand, *Cal-A*@OSN(110), an enzyme–silica composite synthesized under the highest EtOH concentration, showed a pH profile with relatively higher pH values compared to *Cal-A*@OSN(0), in which the pH approached 10.5 at the maximum, which is indicative of a significant effect of EtOH on enzyme structures during the synthesis.

To check the structural stability of *Cal-A* after the immobilization within the OSNs, the FTIR spectra of *Cal-A*@OSN(0) and

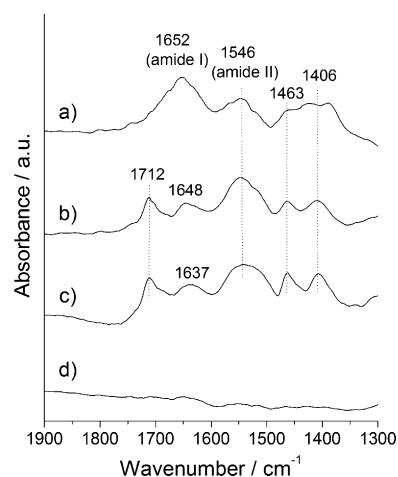


Figure 2. FTIR spectra of a) native *Cal-A*, b) *Cal-A*@OSN(0), c) *Cal-A*@OSN(110), and d) *Cal-A*@OSN(0) calcined at 700 °C in air.

Cal-A@OSN(110) were recorded and compared with that of native *Cal-A*. As shown in Figure 2, native *Cal-A* demonstrated several characteristic absorption bands; the bands seen at 1546 cm^{-1} is assigned to the bending and stretching modes of the N–H and C–N bonding of amide groups (amide II) and the band at 1652 cm^{-1} is assigned to the C–O stretching of the α -helical conformation of *Cal-A* molecules (amide I).^[10,49] The peak intensities and positions of these amide bands are typically used for the determination of the conformation and unfolding of the proteins.^[50] The bands seen in the range of 1350–1490 cm^{-1} are assigned to the $-\text{CH}_2-$ and $-\text{CH}_3$ stretching modes of the aliphatic moieties of amino acid side chains of enzymes.^[10,49] The FTIR spectra of *Cal-A*@OSN(0) and *Cal-A*@OSN(110) also demonstrated such bands characteristic of the protein structure of *Cal-A* (the bands seen at 1406 and 1463 cm^{-1} may also include those corresponding to the aliphatic chains of OA and APTES) as well as additional bands at 1712 cm^{-1} , which are assignable to the C=O bonding of the carboxylic acid groups of OA. The presence of the amide I and amide II bands confirms the immobilization of enzymes in their structures. Nevertheless, the spectra of *Cal-A*@OSN(0) showed distinct shifts of the amide I band toward 4 cm^{-1} lower wave numbers (from 1652 to 1648 cm^{-1}) with a decreased intensity (Figure 2b). Our precedent study has confirmed that enzymes are selectively sequestered within the silica matrix of the shell, not in the oil phase.^[43] Thus, the protein structures of *Cal-A* are found to be perturbed by the confinement inside the silica matrix and do not have space for changing their structural conformations. This shift was most distinctly appeared in the spectrum of *Cal-A*@OSN(110) with a 15 cm^{-1} shift (from 1652 to 1637 cm^{-1}), which suggests an extensive conformational change of enzymes upon the immobilization because of the addition of EtOH (Figure 2c). Notably, no specific absorption bands were observed for *Cal-A*@OSN materials calcined at 700 °C in air, which confirms that the above specific bands are all attributable to the organic contents, not to the silica matrix (Figure 2d). These results confirm the immobilization of *Cal-A* molecules inside the silica matrix

of the OSN and its strong confinement effect whereas the molecular configuration of the immobilized enzymes is likely deformed upon the immobilization, depending on the amount of EtOH added.

Effect of EtOH on OSN structures

The morphological features of the *Cal-A*@OSN materials were observed by using the combined SEM and TEM analysis. The left panel of Figure 3 shows the SEM images of *Cal-A*@OSN materials synthesized with varied EtOH concentrations. The SEM image of *Cal-A*@OSN(0) confirms that it is composed of highly dispersed spherical nanoparticles with an average particle size (determined based on the sizes of 200 particles for each data) of approximately 230 nm (Figure 3 a). Although *Cal-A*@OSN(50) provided an average particle size similar to that of *Cal-A*@OSN(0), the samples prepared with higher EtOH concentrations—*Cal-A*@OSN(70) and *Cal-A*@OSN(110)—showed increased average particle sizes, 241 and 263 nm, respectively (Figure 3 c and d). As an unusual case, some nanoparticles with a wrinkled surface morphology were observed for *Cal-A*@OSN(110) (Figure 3 d) whereas other materials showed perfect spherical morphologies. The final size/shape of the OSN materials are, in principle, determined by the ones of the oil phase (OA); hence, it can be assumed that EtOH affects the size/shape of the oils by reducing the surface tension and changing the curvature of OA micelles.^[44]

The TEM images of *Cal-A*@OSN materials are shown in the right panel of Figure 3, which indicate that *Cal-A*@OSN materials include not only monodispersed spherical particles but also some polydispersed/aggregated particles and some particles with a size smaller than 100 nm. All samples showed clear contrasts between cores and shell layers in the TEM images. Thermogravimetric data of *Cal-A*@OSN(0) measured in air flow showed 29.5 % weight loss at ≥ 210 °C, which is ascribed to the combustion of organic contents, such as OA, enzymes, and aminopropyl groups of APTES (Figure S1). Considering the composition of the initial reaction solution, this weight loss is mostly due to the combustion of OA. Furthermore, such core-shell structures had been retained even after calcination at 700 °C in air (Figure S2). These results confirm that the core cavities of these materials are occupied by OA, which is covered with shell layers made of silica. Along with the addition of increased amount of EtOH, the thickness of the silica shell layer decreased unambiguously; the shell thickness of *Cal-A*@OSN(0) was estimated to be 16–20 nm and the one of *Cal-A*@OSN(110) was estimated to be 8–12 nm from the TEM images (cf. Figure 3 a and d). This is most likely due to the inverse relationship between the particle size and the silica shell thickness; that is, the larger the OSN particle, the thinner the silica shell. Considering the fact that the molecular dimensions of *Cal-A* calculated from crystallographic data are approximately 6.3×5.6×4.2 nm (although the dimensions in the solution and the immobilized state may differ from the crystallographic dimensions),^[28,51] it is suggested that the *Cal-A* molecules embedded in the thinner silica shell of *Cal-A*@OSN(110) are most likely surface exposed, whereas the thick silica shell of *Cal-*

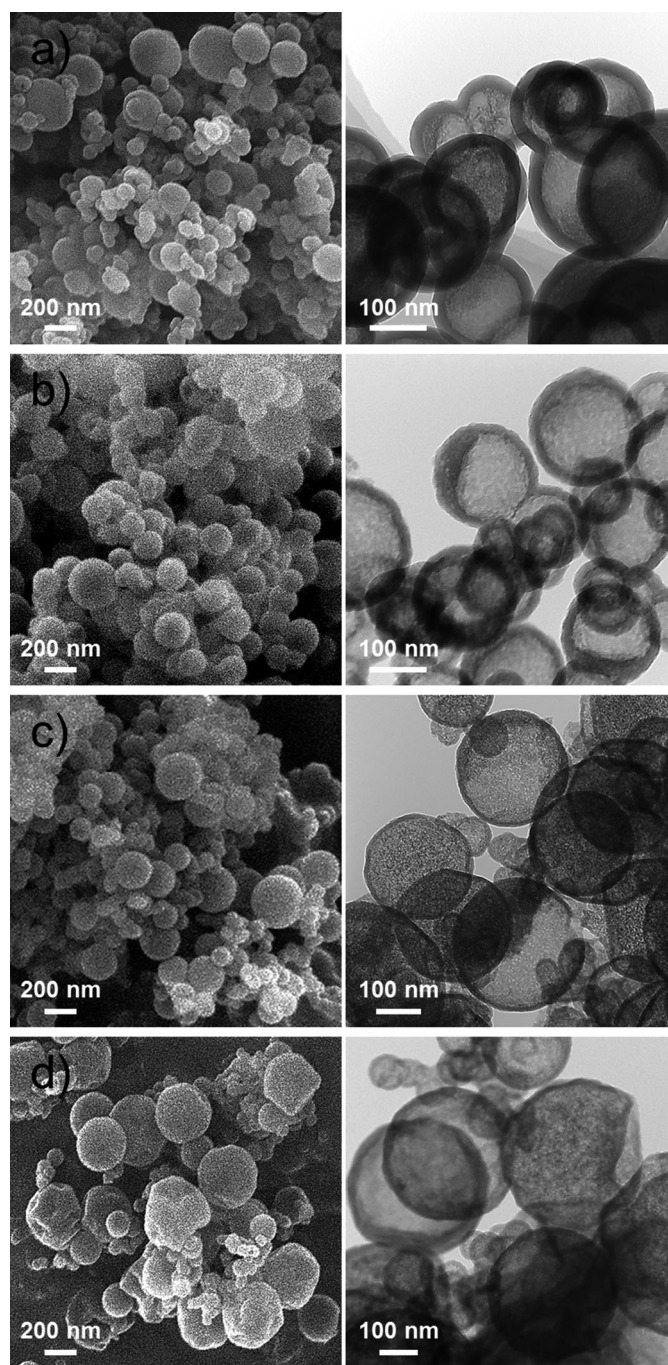


Figure 3. SEM (left) and TEM (right) micrographs of *Cal-A*@OSN synthesized with varied EtOH/OA ratios: a) 0, b) 50, c) 70, and d) 110.

A@OSN(0) can sufficiently accommodate *Cal-A* molecules in its silica matrix. This difference in geometric dimensions would affect the stability and recyclability of the embedded enzyme species, as discussed later.

The existence of mesopores in the silica shell was not observed in the TEM images probably owing to a relatively disordered, random orientation of the pores^[43] but was instead confirmed by using XRD analysis. The XRD patterns of the as-synthesized *Cal-A*@OSN materials and those calcined at 700 °C in air are shown in Figure 4 a and b, respectively. The as-synthe-

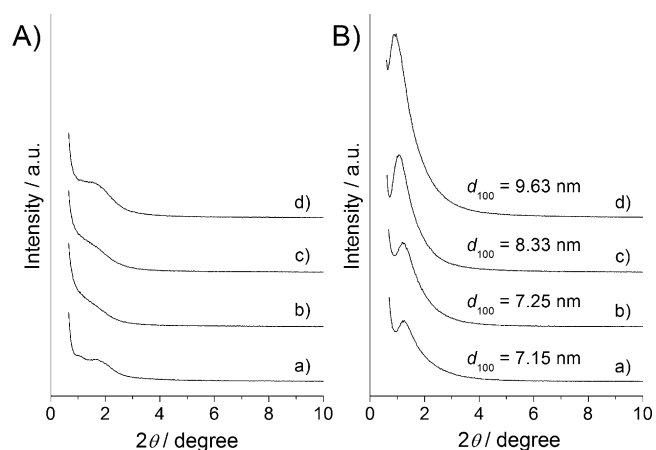


Figure 4. XRD patterns of A) as-synthesized *Cal-A@OSN* materials synthesized with varied EtOH/OA ratios—a) 0, b) 50, c) 70, and d) 110—and B) those calcined at 700 °C in air.

sized *Cal-A@OSN* materials showed no diffraction peaks in the low-angle region of XRD patterns because of the filling of the pores with OA (Figure 4a). On the other hand, the materials calcined at 700 °C in air showed clear diffraction peaks at approximately 0.92–1.23°, which are indexed as the (100) reflection typical of wormhole-like mesopore structures (Figure 4b). These are the mesopores created through the self-assembly of OA as an anionic surfactant.^[44] With an increase in the amount of EtOH added, these peaks appeared more clearly and *d*-spacing values increased correspondingly from 7.15 to 9.63 nm, which suggests a substantial change in the mesoporosity of the silica shell.

The pore characteristics of the samples were further characterized by using nitrogen physisorption analysis. The nitrogen adsorption–desorption isotherms of the *Cal-A@OSN* materials are shown in Figure 5. The nitrogen adsorption isotherms of the as-synthesized *Cal-A@OSN* materials demonstrated typical type III isotherms according to the IUPAC classification, and the sum of micropore and mesopore volumes (V_{pore}) was negligible (<0.06) in all cases, which indicates that they are nonporous solids. After the calcination treatment at 700 °C in air, the adsorbed nitrogen quantities increased appreciably owing to the loss of organic contents, and the nitrogen sorption isotherms showed type II isotherms with broad hysteresis loops at $P/P_0 = 0.5–1.0$, which correspond to the mesopores in the silica shells.

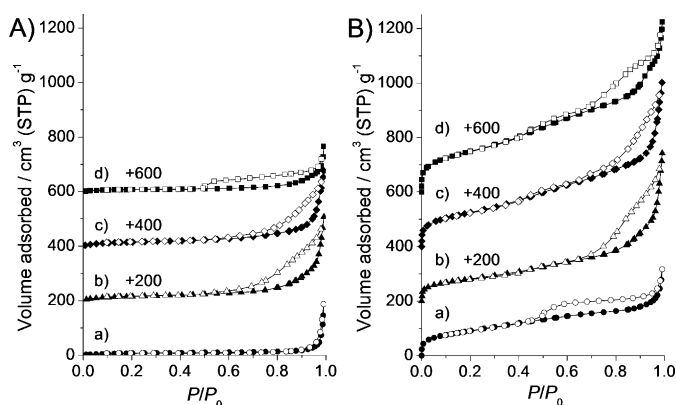


Figure 5. N₂ adsorption–desorption isotherms of A) as-synthesized *Cal-A@OSN* materials synthesized with varied EtOH/OA ratios—a) 0, b) 50, c) 70, and d) 110—and B) those calcined at 700 °C in air. Filled and empty symbols represent adsorption and desorption branches, respectively.

The steep increases in the isotherms at $P/P_0 > 0.90$ are due to the filling of the hollow cavities and the interparticle voids caused by particle aggregation. This type of isotherm is in agreement with the presence of a hierarchical porosity organization of the mesoporous silica hollow spheres, as reported previously.^[44] The textural parameters obtained from nitrogen adsorption isotherms are summarized in Table 1. The calcined *Cal-A@OSN(0)* was found to have a BET surface area of 325 m²g^{−1} and a total pore volume of 0.472 cm³g^{−1}, whereas the as-synthesized *Cal-A@OSN(0)* demonstrated quite low structural parameters (Table 1). These structural parameters apparently increased along with the addition of EtOH in the synthesis medium; the specific surface area of the calcined materials increased linearly from 325 to 540 m²g^{−1}. The increase in surface area is attributable to the densification of the pores in the silica shells, which can be confirmed from the increased peak intensities of the (100) reflections in XRD patterns as well (Figure 4b). The total pore volume increased from 0.472 to 0.933 cm³g^{−1} and thus the micropore/mesopore volume increased from 0.29 to 0.44 cm³g^{−1} with the increase in the EtOH/OA ratio up to 110. Considering that the total pore volume includes micropore/mesopore volumes and cavity volumes within the hollow spheres (as well as interparticle voids caused by particle aggregation), it is suggested that the *Cal-A@OSN* materials synthesized with higher EtOH concentrations

Table 1. Textural properties of *Cal-A@OSN* materials synthesized with 1 OA/1 APTES/6.7 TEOS/XEtOH/1600 H₂O.

Sample	XEtOH	Enzyme loading ^[a] [mg _{enzyme} g _{cat} ^{−1}]	Average particle size ^[b] [nm]	Silica shell thickness ^[c] [nm]	As-synthesized				After calcination			
					$S_{\text{BET}}^{\text{[d]}}$ [m ² g ^{−1}]	$V_{\text{total}}^{\text{[e]}}$ [cm ³ g ^{−1}]	$V_{\text{pore}}^{\text{[f]}}$ [cm ³ g ^{−1}]	$D_p^{\text{[g]}}$ [nm]	$S_{\text{BET}}^{\text{[d]}}$ [m ² g ^{−1}]	$V_{\text{total}}^{\text{[e]}}$ [cm ³ g ^{−1}]	$V_{\text{pore}}^{\text{[f]}}$ [cm ³ g ^{−1}]	$D_p^{\text{[g]}}$ [nm]
<i>Cal-A@OSN(0)</i>	0	18.9	231	16–20	26	0.284	< 0.01	n.d.	325	0.472	0.29	4.2
<i>Cal-A@OSN(50)</i>	50	18.8	224	11–16	58	0.455	0.05	n.d.	391	0.866	0.32	3.7
<i>Cal-A@OSN(70)</i>	70	18.4	241	10–15	57	0.411	0.05	n.d.	452	0.926	0.35	3.4
<i>Cal-A@OSN(110)</i>	110	18.4	263	8–12	26	0.236	0.06	4.0	540	0.933	0.44	3.4

[a] Determined by subtracting the amount of enzyme remained in the supernatant solution from the initial amount of enzyme added; [b] Determined by SEM observations; [c] Determined by TEM observations; [d] Specific surface area calculated by using the BET method; [e] Total pore volume at $P/P_0 = 0.99$; [f] Volume of pores including micropores and mesopores; [g] Pore diameter estimated by using the BJH method and the N₂ desorption branch.

possess silica shells with higher porosities and cores with larger cavity spaces.

The addition of EtOH also caused substantial changes in pore sizes and their distributions. Pore size distribution curves calculated by using the BJH method with desorption branches of the N_2 isotherms are shown in Figure 6. As expected, the as-synthesized *Cal-A*@OSN materials demonstrated no clear pore distributions owing to their nonporous nature (Figure 6a). On

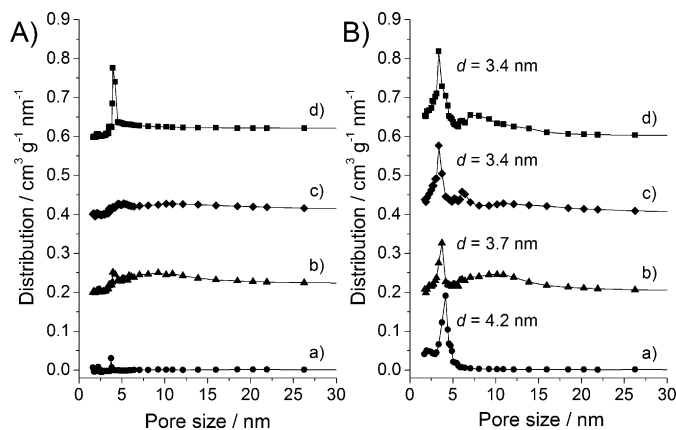


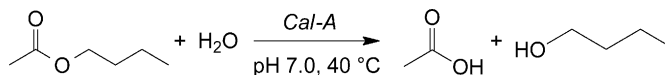
Figure 6. Pore size distributions of A) as-synthesized *Cal-A*@OSN materials synthesized with varied EtOH/OA ratios—a) 0, b) 50, c) 70, and d) 110—and B) those calcined at 700 °C in air calculated by using the BJH method with the desorption branch of the N_2 isotherm.

the other hand, the calcined *Cal-A*@OSN materials showed distinct pore distributions centered at approximately 3.4–4.2 nm (Figure 6b), which again confirms that these samples have defined mesoporous structures. The pore size of the calcined *Cal-A*@OSN(0) was determined to be 4.2 nm and decreased to 3.7, 3.4, and 3.4 nm with the increase in the EtOH/OA ratio to 50, 70, and 110, respectively. This is due to the fact that EtOH reduces the surface tension of OA dramatically and affects the packing of OA in micelles.^[44] More importantly, the samples prepared by adding EtOH demonstrated secondary pores in the pore size range of 5–20 nm (Figure 6B, curve b and curve d). The origin of the creation of these secondary pores, that is, whether they are caused by different micelle formations induced by adding EtOH or they are the voids caused by the removal of enzyme molecules through calcination,^[52] still remains unclear; however, the former may be a valid reason because such pores were not observed in the sample prepared without adding EtOH (Figure 6B, curve a).

These combined analyses revealed that the addition of EtOH to the initial synthesis medium yields *Cal-A*@OSN with larger particle sizes and results in the formation of thinner, highly porous silica shells with both defined mesopores and secondary mesopores compared to the material synthesized without adding EtOH because EtOH can reduce the surfactant packing parameter g .^[44] As an exceptional case, the silica shell morphology changed from a perfect spherical shape to a wrinkled surface morphology upon the addition of an excess of EtOH (EtOH/OA > 110).

Enzyme activity assay

The enzyme activity of the *Cal-A*@OSN materials was assessed by using the hydrolysis of *n*-butyl acetate in the phosphate buffer (pH 7.0) as a test reaction (Scheme 2) and was compared with the activity of the free enzyme.



Scheme 2. Hydrolysis of *n*-butyl acetate.

The reaction profiles of the *Cal-A*@OSN materials as well as that of the free enzyme are shown in Figure 7a, in which the enzyme dosage was kept constant (1.0 mg of *Cal-A*) and the enzyme activity was compared on the basis of the yields of *n*-butanol. As shown in Figure 7a, *Cal-A*@OSN(0) showed as high a reaction rate as that of free *Cal-A*, with a > 99% stoichiometric yield of *n*-butanol after 6 h of the reaction time, which indi-

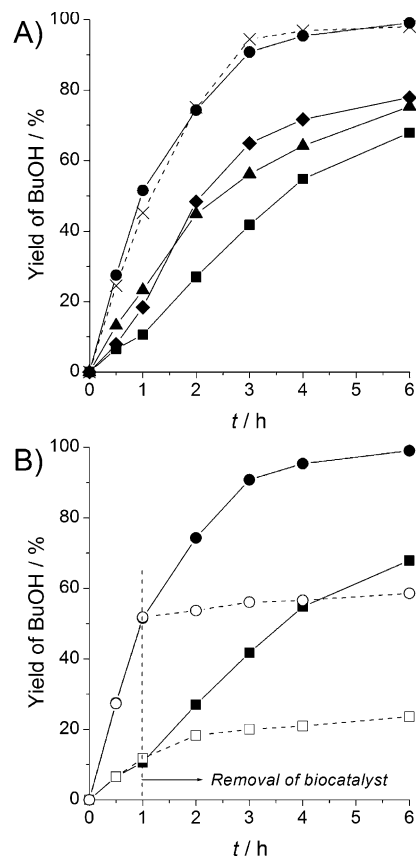


Figure 7. A) Reaction profiles obtained during the hydrolysis of *n*-butyl acetate catalyzed by free *Cal-A* (x), *Cal-A*@OSN(0) (●), *Cal-A*@OSN(50) (▲), *Cal-A*@OSN(70) (◆), and *Cal-A*@OSN(110) (■). B) Comparison of reaction profiles obtained during the hydrolysis of *n*-butyl acetate catalyzed by *Cal-A*@OSN(0) (●, ○) and *Cal-A*@OSN(110) (■, □). Filled symbols: without removal of biocatalysts; empty symbols: with removal of biocatalysts through filtration of the reaction mixtures (the reaction had previously been allowed to proceed for 1 h). Reaction conditions: Biocatalyst (including 1.0 mg of *Cal-A*), *n*-butyl acetate aqueous solution (50 mM, 1 mL), sodium phosphate buffer (50 mM, 9 mL), pH 7.0, 40 °C, and reaction time 6 h.

cates an excellent retention of its enzyme activity upon immobilization. This is probably due to the combination of the ambient synthetic conditions that preserve the inherent activity of enzymes and an optimized configuration of enzymes in the vicinity of the reactive surface that maximizes the contact between enzymes and reactants. In contrast, the *Cal-A*@OSN materials synthesized by adding EtOH demonstrated much slower reaction rates than *Cal-A*@OSN(0), and the initial reaction rate decreased in the following order: *Cal-A*@OSN(0) > *Cal-A*@OSN(50) > *Cal-A*@OSN(70) > *Cal-A*@OSN(110), yet they retained most of their activities. Considering the fact that the enzyme loadings are the same in all samples, this decreased activity can be associated with the denaturation of enzymes during the synthesis, as confirmed by the pH profiles and the FTIR spectra (Figures 1 and 2). One could hypothesize that the reaction kinetics may be affected by the diffusion effect of the reactants; however, as confirmed above, the addition of a larger amount of EtOH affords *Cal-A*@OSN materials with thinner, highly porous silica shells, which should, in principle, contribute to an efficient access of the reactants to enzymes and thus discounts this possibility.

A strong relationship between the pore characteristics of the silica shells and the residual enzyme activities exists. The reaction profiles obtained during the hydrolysis of *n*-butyl acetate over *Cal-A*@OSN(0) and *Cal-A*@OSN(110) with and without the removal of biocatalysts through filtration of the reaction mixtures are compared in Figure 7b. When *Cal-A*@OSN(0) was used as a biocatalyst, the reaction was quenched immediately after the recovery of the particles from the reaction mixture through simple filtration, which demonstrated a robust immobilization of enzymes within the OSN support. On the other hand, *Cal-A*@OSN(110) showed a modest increase in the *n*-butanol yield even after the recovery of the particles [*n*-butanol yield: 11.8% (1 h) → 23.6% (6 h)], which indicates a leaching of some fractions of the enzymes into the reaction solution during its use. Similar reaction kinetics were observed for *Cal-A*@OSN(50) and *Cal-A*@OSN(70) (data not shown). On the basis of the detailed structural characterizations disclosed above, the leaching of enzymes can be associated with the thin silica shell and/or the high porosity of the silica shell; that is, the enzymes immobilized within such permeable silica shells are considered to be partly surface exposed and loosely bound, which thus results in an easy elution of enzymes. Such a hypothesis is also confirmed by using a recycling test, as demonstrated in the following section.

Recycling assay

Relative enzyme activities of the *Cal-A*@OSN biocatalysts over 10 reaction cycles in the hydrolysis of *n*-butyl acetate, in which the same amount of the biocatalyst (50 mg) was used for each catalytic run to show the degree of enzyme leaching, are shown in Figure 8. The *Cal-A*@OSN(0) biocatalyst, which was proven to be the most efficient biocatalyst that we examined, could be repeatedly used at least 10 times without appreciable loss of its activity (>98% relative to the initial activity had been retained even after 10 cycles), which demonstrates its ex-

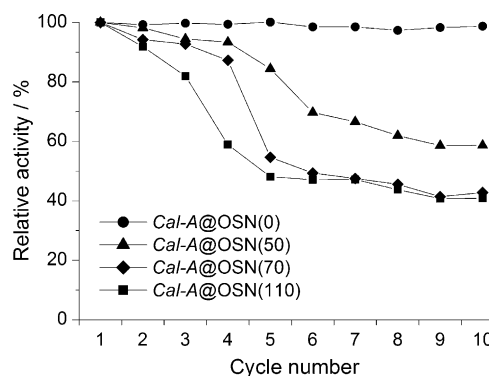


Figure 8. Recyclability of *Cal-A*@OSN biocatalysts. Reaction conditions: biocatalyst (50 mg), *n*-butyl acetate aqueous solution (50 mM, 1 mL), sodium phosphate buffer (50 mM, 9 mL), pH 7.0, 40 °C, and reaction time 6 h.

cellent recyclability. This may be the consequence of the robust confinement effect of the thick, dense silica matrix of *Cal-A*@OSN(0), which enables the prevention of the undesired leaching of enzymes. In contrast, *Cal-A*@OSN(50), *Cal-A*@OSN(70), and *Cal-A*@OSN(110) lost large parts of their enzyme activities during their first five to six cycles, followed by modest decreases; although *Cal-A*@OSN(50) still retained approximately 60% of its enzyme activity after 10 cycles of the reaction, *Cal-A*@OSN(70) and *Cal-A*@OSN(110) lost more than a half of their initial activities during the same number of cycles, which show poorer recyclabilities. Considering the overall trend seen in Figures 7 and 8, the reduction in enzyme activity and recyclability can be associated with the subpar structural properties of the silica shells (i.e., the thinner the silica shell and the higher the silica shell porosity, the higher the degree of enzyme leaching), which thereby leads to a continual leaching of enzymes into reaction solutions during their first several cycles. Enzymes could possibly be leached through the secondary pores, the diameters of which are sufficiently wider than the molecular dimensions of the enzymes, as confirmed by the structural analysis (see Figure 6); such a leaching was hardly observed for *Cal-A*@OSN(0), which has no secondary pores.

Stability assay

In addition to the recyclability of enzymes, the thermal/chemical stability is of key importance for their practical biotechnological applications because the ability to retain enzyme activity in wide pH ranges and at high temperatures provides a number of processing advantages such as improved reaction rate and substrate solubility, which enables the efficient catalysis of enzymes.

To assess the thermal/chemical stability of the *Cal-A*@OSN biocatalysts, some selected biocatalysts were subjected to the hydrolysis of *n*-butyl acetate at different solution temperatures and pH values, in which the activities were normalized by that of free *Cal-A* at pH 7.0 and 40 °C. As shown in Figure 9A and B, the free enzyme in the buffer solution was readily denatured and lost most of its activity at ≥ 60 °C or under extreme pH

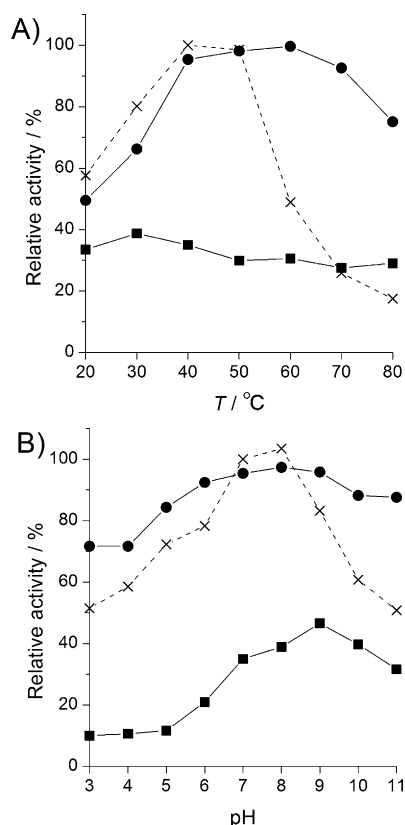


Figure 9. Enzyme activity of *Cal-A*@OSN(0) (●), *Cal-A*@OSN(110) (■), and native *Cal-A* (x) at different a) temperature and b) pH values. The activities were normalized by that of free *Cal-A* at pH 7.0 and 40 °C. Reaction conditions: biocatalyst (including 1.0 mg of *Cal-A*), *n*-butyl acetate aqueous solution (50 mM, 1 mL), buffer solution (50 mM, 9 mL), and reaction time 2 h.

conditions. In contrast, *Cal-A*@OSN(0) retained most of its activity over wide temperature and pH ranges, especially at ≥ 60 °C, which proves its improved thermal/chemical stability. This improved stability can be associated with the robust stabilizing effect of the thick and rigid silica matrix of the shell (see above). Compared to such a tightly immobilized enzyme–silica composite, the *Cal-A*@OSN(110) biocatalyst with a thinner and more permeable silica shell showed a limited thermal/chemical stability of the enzymes under most of the conditions examined. This is primarily because of the harsh synthesis conditions applied, which reduce the residual activity of enzymes (Figures 1 and 2) and secondarily because of the poor stabilizing effect of the silica shell of *Cal-A*@OSN(110); the latter factor leads to a substantial leaching of enzymes during the reaction and extensive conformational changes typical of thermal/chemical denaturation, which therefore results in markedly low relative activities under the harsh reaction conditions. These findings elucidate again that a silica shell with optimized shell thickness and porosity offers a robust confinement effect of enzymes, which thereby limits the undesired denaturation/leaching of enzymes, and accordingly providing thermal/chemical stability necessary for enzymes to retain their activities even under harsh conditions.

Effect of OA on enzyme activity

Another important factor that needs to be examined is the effect of the presence of oil (OA) on the enzyme activity. In our precedent study, it was demonstrated that this enzyme–silica composite could act as an efficient, reusable, and stable biocatalyst in the catalysis in an organic solvent (in *n*-heptane) whereas native enzyme alone was found to be inactive under the same reaction conditions,^[43] which implies a productive role of OA in the catalysis. However, the question of whether the presence of oil in the core is truly favorable for catalysis requires elucidation. A pertinent result is provided by a comparative testing with *Cal-A*@OSN(0) and OA-extracted *Cal-A*@OSN(0). The reaction profiles of *Cal-A*@OSN(0) and OA-extracted *Cal-A*@OSN(0) in the hydrolysis of *n*-butyl acetate in the phosphate buffer (pH 7.0) are shown in Figure 10. Most of

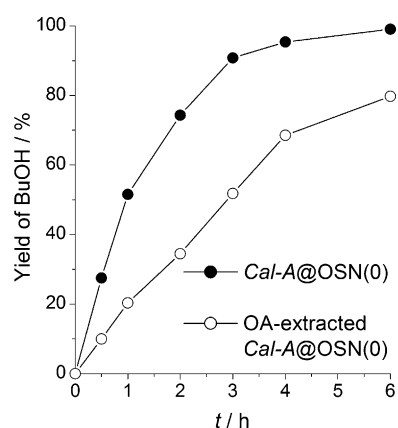


Figure 10. Effect of the presence of oil (OA) on the enzyme activity of *Cal-A*@OSN(0) biocatalyst. Reaction conditions: biocatalyst (including 1.0 mg of *Cal-A*), *n*-butyl acetate aqueous solution (50 mM, 1 mL), sodium phosphate buffer (50 mM, 9 mL), pH 7.0, 40 °C, and reaction time 6 h.

the oil (OA) was removed from the particles by treating with *n*-heptane at 40 °C while retaining the enzyme structure, and enzyme dosage in the reaction mixture was kept constant (1.0 mg of *Cal-A*). As shown in Figure 10, OA-extracted *Cal-A*@OSN(0) apparently showed a slower reaction rate than pristine *Cal-A*@OSN(0). A similar result was observed in the hydrolysis of tricaprilyn ($C_{27}H_{50}O_6$) in water-saturated *n*-heptane (Figure S3), which confirms that the OA in the core plays an important role in achieving a high catalytic efficiency in both organic and water phase reactions. A plausible reason for this is an amphiphilic environment on the reactive surface induced by oil-filled core–shell structure, which facilitates the access of organic substrates dissolved in water to the active sites of enzymes in the water phase reaction and increases the affinity with the organic media in the organic phase reaction, and thus leads to the effective catalytic efficiencies.

Conclusions

Candida antarctica lipase A (*Cal-A*) was immobilized on oil-filled spherical silica nanoparticles (OSNs) with different silica

shell structures through an anionic surfactant-induced self-assembly approach and using EtOH as a cosolvent. The addition of EtOH to the initial synthesis medium yielded *Cal-A@OSN* with larger particle sizes and resulted in the formation of thinner, highly porous silica shells with both defined mesopores (3.4–4.2 nm) and secondary mesopores (5–20 nm) compared to the material synthesized without adding EtOH because EtOH can reduce the surfactant packing parameter g . The retention of the enzyme activity during biocatalysis was affected significantly by the structural properties of the silica shells (thickness and porosity), and it was found that a dense silica shell with a thickness sufficiently larger than the molecular dimensions of enzymes is essential to yield an active, recyclable, and stable biocatalyst. Further optimization of the silica shell thickness, for example, through the addition of extra silicon sources such as TEOS, has not been developed here; however, additional studies focused on this aspect would be needed in the future to obtain high-performance heterogeneous biocatalyst combining a maximized catalytic efficiency of enzymes and an enhanced recyclability preferably over hundreds to thousands of cycles. Furthermore, oleic acid encapsulated within the core cavity of *Cal-A@OSN* was found to play an important role in achieving a high catalytic efficiency probably by inducing an amphiphilic environment on the reactive surface. This study demonstrated several close relationships between the structures of the support and the performances of the immobilized enzymes, which would provide important insights into the strategy for designing high-performance enzyme–silica composite biocatalysts, which combines high catalytic efficiency, recyclability, and stability.

Experimental Section

Materials

Cal-A (EC 3.1.1.3; $\geq 1.0 \text{ U mg}^{-1}$) and APTES were purchased from Sigma–Aldrich and used without any further purification. OA and TEOS were purchased from Nacalai Tesque, Inc., and used as such. All commercially available organic compounds for catalytic reactions were purified by using standard methods.

Synthesis of *Cal-A@OSN*

The synthesis of *Cal-A@OSN* materials with different silica shell structures was performed according to the method reported previously but with a few minor modifications.^[43] In a typical synthesis, OA (0.282 g, 99%, 1 mmol) was dispersed in the aqueous solution (60 mL) containing the desired amount of EtOH (99.5%) with vigorous stirring. The mixture was then sonicated for 1 min. *Cal-A* (14 mg) was dispersed into this solution, and then a mixture containing TEOS (1.40 g, 98%, 6.7 mmol) and APTES (0.221 g, 99%, 1 mmol) was added dropwise with stirring. The solution was stirred magnetically for approximately 10 min at RT, left to age for 2 h at the same temperature under static conditions, and aged for another 24 h at 50 °C to form the silica network. The initial molar composition was adjusted to 1 OA/1 APTES/6.7 TEOS/ X EtOH/1600 H₂O, in which the molar ratio of EtOH/OA (X) was varied from 0 to 110. The resultant suspension was centrifuged at 20 000g, washed twice with distilled water, filtered, and dried overnight under vacuum to

afford *Cal-A@OSN(X)*, in which X represents the molar ratio of EtOH/OA. The prepared samples were stored in the refrigerator at 4 °C until use to circumvent denaturation. The loading amount of the enzyme in the sample was determined by subtracting the amount of the enzyme remained in the supernatant solution, which was spectroscopically determined with a Shimadzu UV-2450 spectrophotometer, from the initial amount of the enzyme added.

Characterization

The FTIR spectra were recorded on a JASCO FT/IR-6100 instrument in the spectral range of 2000–400 cm⁻¹ under vacuum with a resolution of 4 cm⁻¹. Field-emission SEM images were recorded on JEOL JSM-6500F. TEM images were obtained with a Hitachi HF-2000 FE-TEM equipped with a Kevex energy-dispersive X-ray detector operated at 200 kV. The sample was suspended in EtOH using ultrasound, and then a droplet of the suspension was dried on a carbon grid. The powder XRD patterns were recorded on a Rigaku Ultima IV diffractometer with CuK α radiation ($\lambda = 1.54056 \text{ \AA}$) at $2\theta = 0.6\text{--}10.0^\circ$. Nitrogen adsorption–desorption isotherms were measured at -196°C with the BELSORP-max system (BEL Japan). Enzyme-loaded samples were outgassed at 80 °C for at least 12 h to vaporize physisorbed water, whereas calcined samples were outgassed at 350 °C for 3 h before the measurements. Specific surface area was calculated by using the BET method with nitrogen adsorption data at $P/P_0 = 0.05\text{--}0.35$. The pore size distribution was obtained by using the BJH method and the desorption branch of the N₂ isotherm. Thermogravimetric analysis was performed by using TG-DTA 2000S (MAC Science Co. Ltd.) from RT to 800 °C at a heating rate of 10 °C min⁻¹ in the air flow of 50 cm³ min⁻¹.

Enzyme activity assay

The enzyme activity of the enzyme–silica composites was assessed by using the hydrolysis reaction of *n*-butyl acetate. In a typical method, the reaction was initiated by adding *n*-butyl acetate aqueous solution (1 mL, 50 mM) into the mixture of the buffer solution (9 mL, 50 mM; sodium acetate for pH 3.0–5.0, sodium phosphate for pH 6.0–8.0, and Gly-NaOH for pH 9.0–11.0) and the biocatalyst containing *Cal-A* (1.0 mg), which had been preincubated at 40 °C. The reaction mixture was stirred magnetically at 40 °C for 6 h. A portion of the reaction mixture was taken at appropriate intervals through filtration and then analyzed by using GC (Shimadzu GC-14B) with a flame ionization detector equipped with a Porapak Q column. The solid catalysts were recovered through centrifugation (5 min at 20 000g) after the reaction, washed thrice with deionized water, and subjected to the next catalytic run.

Acknowledgements

This work was financially supported by the Grant-in-Aid for Scientific Research (KAKENHI) in Priority Area “Molecular Nano Dynamics” from the Ministry of Education, Culture, Sports, Science and Technology of Japan (no. A233603560). The authors are grateful to Dr. Eiji Taguchi and Prof. Hiroto Mori at the Research Center for Ultra-High Voltage Electron Microscopy, Osaka University, for assistance with TEM measurements. Y.K. thanks the JSPS Research Fellowships for Young Scientists.

Keywords: biocatalysis · enzymes · heterogeneous catalysis · silicates · structure–activity relationships

- [1] a) C. T. Kresge, M. E. Leonowicz, W. J. Roth, J. C. Vartuli, J. S. Beck, *Nature* **1992**, *359*, 710–712; b) J. S. Beck, J. C. Vartuli, W. J. Roth, M. E. Leonowicz, C. T. Kresge, K. D. Schmitt, C. T.-W. Chu, D. H. Olson, E. W. Sheppard, S. B. McCullen, J. B. Higgins, J. L. Schlenker, *J. Am. Chem. Soc.* **1992**, *114*, 10834–10843.
- [2] a) P. T. Tanev, T. J. Pinnavaia, *Science* **1995**, *267*, 865–867; b) S. A. Bagshaw, E. Prouzet, T. J. Pinnavaia, *Science* **1995**, *269*, 1242–1244.
- [3] D. Zhao, J. Feng, Q. Huo, N. Melosh, G. H. Fredrickson, B. F. Chmelka, G. D. Stucky, *Science* **1998**, *279*, 548–552.
- [4] A. Corma, *Chem. Rev.* **1997**, *97*, 2373–2420.
- [5] J. Y. Ying, C. P. Mehnert, M. S. Wong, *Angew. Chem.* **1999**, *111*, 58–82; *Angew. Chem. Int. Ed.* **1999**, *38*, 56–77.
- [6] S. Okada, K. Mori, T. Kamegawa, M. Che, H. Yamashita, *Chem. Eur. J.* **2011**, *17*, 9047–9051.
- [7] a) Y. Kuwahara, K. Nishizawa, T. Nakajima, T. Kamegawa, K. Mori, H. Yamashita, *J. Am. Chem. Soc.* **2011**, *133*, 12462–12465; b) Y. Kuwahara, D.-Y. Kang, J. Copeland, N. A. Brunelli, S. A. Didas, P. Bollini, C. Sievers, T. Kamegawa, H. Yamashita, C. W. Jones, *J. Am. Chem. Soc.* **2012**, *134*, 10757–10760.
- [8] E. Katz, I. Willner, *Angew. Chem.* **2004**, *116*, 6166–6235; *Angew. Chem. Int. Ed.* **2004**, *43*, 6042–6108.
- [9] C. Ispas, I. Sokolov, S. Andreescu, *Anal. Bioanal. Chem.* **2009**, *393*, 543–554.
- [10] M. Hartmann, *Chem. Mater.* **2005**, *17*, 4577–4593.
- [11] S. Hudson, J. Cooney, E. Magner, *Angew. Chem.* **2008**, *120*, 8710–8723; *Angew. Chem. Int. Ed.* **2008**, *47*, 8582–8594.
- [12] H. H. P. Yiu, P. A. Wright, *J. Mater. Chem.* **2005**, *15*, 3690–3700.
- [13] H. H. P. Yiu, C. H. Botting, N. P. Botting, P. A. Wright, *Phys. Chem. Chem. Phys.* **2001**, *3*, 2983–2985.
- [14] C. Lei, Y. Shin, J. Liu, E. J. Ackerman, *J. Am. Chem. Soc.* **2002**, *124*, 11242–11243.
- [15] a) A. Salis, D. Meloni, S. Ligas, M. F. Casula, M. Monduzzi, V. Solinas, E. Dumitriu, *Langmuir* **2005**, *21*, 5511–5516; b) A. Salis, M. F. Casula, M. S. Bhattacharyya, M. Pinna, V. Solinas, M. Monduzzi, *ChemCatChem* **2010**, *2*, 322–329.
- [16] P. H. Pandya, R. V. Jasra, B. L. Newalkar, P. N. Bhatt, *Microporous Mesoporous Mater.* **2005**, *77*, 67–77.
- [17] Y. Kuwahara, T. Yamanishi, T. Kamegawa, K. Mori, H. Yamashita, *J. Phys. Chem. B* **2011**, *115*, 10335–10345.
- [18] C. Li, J. Liu, X. Shi, J. Yang, Q. Yang, *J. Phys. Chem. C* **2007**, *111*, 10948–10954.
- [19] E. Serra, E. Díez, I. Díaz, R. M. Blanco, *Microporous Mesoporous Mater.* **2010**, *132*, 487–493.
- [20] F. Secundo, G. Roda, M. Vittorini, A. Ungureanu, B. Dragoi, E. Dumitriu, *J. Mater. Chem.* **2011**, *21*, 15619–15628.
- [21] a) H. Takahashi, B. Li, T. Sasaki, C. Miyazaki, T. Kajino, S. Inagaki, *Chem. Mater.* **2000**, *12*, 3301–3305; b) H. Takahashi, B. Li, T. Sasaki, C. Miyazaki, T. Kajino, S. Inagaki, *Microporous Mesoporous Mater.* **2001**, *44–45*, 755–762.
- [22] M. Tortajada, D. Ramón, D. Beltrán, P. Amorós, *J. Mater. Chem.* **2005**, *15*, 3859–3868.
- [23] Y. Wang, F. Caruso, *Chem. Mater.* **2005**, *17*, 953–961.
- [24] Y. Urabe, T. Shiomi, T. Itoh, A. Kawai, T. Tsunoda, F. Mizukami, K. Sakaguchi, *ChemBioChem* **2007**, *8*, 668–674.
- [25] a) A. Vinu, V. Murugesan, M. Hartmann, *J. Phys. Chem. B* **2004**, *108*, 7323–7330; b) A. Vinu, V. Murugesan, O. Tangermann, M. Hartmann, *Chem. Mater.* **2004**, *16*, 3056–3065; c) A. Vinu, N. Gokulakrishnan, V. V. Balasubramanian, S. Alam, M. P. Kapoor, K. Ariga, T. Mori, *Chem. Eur. J.* **2008**, *14*, 11529–11538.
- [26] D. Jung, C. Streb, M. Hartmann, *Microporous Mesoporous Mater.* **2008**, *113*, 523–529.
- [27] a) N. Brun, A. Babeau Garcia, H. Deleuze, M. F. Achard, C. Sanchez, F. Durand, V. Oestreicher, R. Backov, *Chem. Mater.* **2010**, *22*, 4555–4562; b) N. Brun, A. Babeau Garcia, M. F. Achard, C. Sanchez, F. Durand, G. Laurent, M. Birot, H. Deleuze, R. Backov, *Energy Environ. Sci.* **2011**, *4*, 2840–2844.
- [28] M. Shakeri, K. Engström, A. G. Sandström, J.-E. Bäckvall, *ChemCatChem* **2010**, *2*, 534–538.
- [29] A. Petri, T. Gambicorti, P. Salvadori, *J. Mol. Catal. B* **2004**, *27*, 103–106.
- [30] R. S. Prakasham, P. R. Likhari, K. Rajyalaxmi, C. Subba Rao, B. Sreedhar, *J. Mol. Catal. B* **2008**, *55*, 43–48.
- [31] Z. Cao, J. Zhang, J. Zeng, L. Sun, F. Xu, Z. Cao, L. Zhang, D. Yang, *Talanta* **2009**, *77*, 943–947.
- [32] N. Hao, H. Wang, P. A. Webley, D. Zhao, *Microporous Mesoporous Mater.* **2010**, *132*, 543–551.
- [33] J. Liu, C. Li, Q. Yang, J. Yang, C. Li, *Langmuir* **2007**, *23*, 7255–7262.
- [34] M. Fujiwara, K. Shiokawa, K. Hayashi, K. Morigaki, Y. Nakahara, *J. Biomed. Mater. Res. Part A* **2007**, *81*, 103–112.
- [35] a) M. Mureseanu, A. Galarneau, G. Renard, F. Fajula, *Langmuir* **2005**, *21*, 4648–4655; b) A. Galarneau, M. Mureseanu, S. Atger, G. Renard, F. Fajula, *New J. Chem.* **2006**, *30*, 562–571; c) A. Galarneau, G. Renard, M. Mureseanu, A. Tournette, C. Biolley, M. Choi, R. Ryoo, F. Di Renzo, F. Fajula, *Microporous Mesoporous Mater.* **2007**, *104*, 103–114.
- [36] A. Macario, M. Moliner, A. Corma, G. Giordano, *Microporous Mesoporous Mater.* **2009**, *118*, 334–340.
- [37] P. Audebert, C. Demaille, C. Sanchez, *Chem. Mater.* **1993**, *5*, 911–913.
- [38] D. Avnir, S. Braun, O. Lev, M. Ottolenghi, *Chem. Mater.* **1994**, *6*, 1605–1614.
- [39] a) K. Kawakami, S. Yoshida, *Biotechnol. Tech.* **1994**, *8*, 441–446; b) K. Kawakami, S. Yoshida, *Biotechnol. Tech.* **1995**, *9*, 701–704; c) K. Kawakami, *Biotechnol. Tech.* **1996**, *10*, 491–494.
- [40] I. Gill, A. Ballesteros, *J. Am. Chem. Soc.* **1998**, *120*, 8587–8598.
- [41] H. R. Luckerift, J. C. Spain, R. R. Naik, M. O. Stone, *Nat. Biotechnol.* **2004**, *22*, 211–213.
- [42] a) S. A. Miller, E. D. Hong, D. Wright, *Macromol. Biosci.* **2006**, *6*, 839–845; b) J. D. Swartz, S. A. Miller, D. Wright, *Org. Process Res. Dev.* **2009**, *13*, 584–589.
- [43] Y. Kuwahara, T. Yamanishi, T. Kamegawa, K. Mori, M. Che, H. Yamashita, *Chem. Commun.* **2012**, *48*, 2882–2884.
- [44] L. Han, C. Gao, X. Wu, Q. Chen, P. Shu, Z. Ding, S. Che, *Solid State Sci.* **2011**, *13*, 721–728.
- [45] Z.-A. Qiao, L. Zhang, M. Guo, Y. Liu, Q. Huo, *Chem. Mater.* **2009**, *21*, 3823–3829.
- [46] R. D. Schmid, R. Verger, *Angew. Chem.* **1998**, *110*, 1694–1720; *Angew. Chem. Int. Ed.* **1998**, *37*, 1608–1633.
- [47] Y. Watanabe, P. Pinsiroadom, T. Nagao, A. Yamauchi, T. Kobayashi, Y. Nishida, Y. Takagi, Y. Shimada, *J. Mol. Catal. B* **2007**, *44*, 99–105.
- [48] O. Kirk, M. W. Christensen, *Org. Process Res. Dev.* **2002**, *6*, 446–451.
- [49] S. Adams, A. M. Higgins, R. A. L. Jones, *Langmuir* **2002**, *18*, 4854–4861.
- [50] K. Griebenow, Y. D. Laureano, A. M. Santos, I. M. Clemente, L. Rodríguez, M. W. Vidal, G. Barletta, *J. Am. Chem. Soc.* **1999**, *121*, 8157–8163.
- [51] D. J. Ericsson, A. Kasrayan, P. Johansson, T. Bergfors, A. G. Sandström, J.-E. Bäckvall, S. L. Mowbray, *J. Mol. Biol.* **2008**, *376*, 109–119.
- [52] T. Shiomi, T. Tsunoda, A. Kawai, S. Matsuura, F. Mizukami, K. Sakaguchi, *Small* **2009**, *5*, 67–71.

Received: January 28, 2013

Revised: March 6, 2013

Published online on April 29, 2013